

Interplay between structure and magnetism in $\text{Ho}_x\text{Pr}_{1-x}$ alloys. II. Resonant x-ray magnetic scattering

A. Vigliante

*Department of Physics, Brookhaven National Laboratory, Upton, New York 11973
and Physics Department, State University of New York at Stony Brook, Stony Brook, New York 11794*

M. J. Christensen

Department of Solid State Physics, Risø National Laboratory, DK-400 Roskilde, Denmark

J. P. Hill

Department of Physics, Brookhaven National Laboratory, Upton, New York 11973

G. Helgesen

Department of Physics, Institutt for Energiteknikk, N-2007 Kjeller, Norway

S. Aa. Sørensen and D. F. McMorrow

Department of Solid State Physics, Risø National Laboratory, DK-400 Roskilde, Denmark

Doon Gibbs

Department of Physics, Brookhaven National Laboratory, Upton, New York 11973

R. C. C. Ward and M. R. Wells

Department of Physics, Oxford University, Oxford, OX1 3PU, United Kingdom

(Received 23 July 1997)

X-ray-scattering techniques have been used to study the crystal and magnetic structures of $\text{Ho}_x\text{Pr}_{1-x}$ alloys in the form of thin films. Three distinct crystal structures are found as a function of concentration x , each of which has a characteristic magnetic structure. For $x \geq 0.6$ a hexagonal-close-packed phase is found with the magnetic moments ordered in a basal-plane helix, whereas for $0.4 \leq x < 0.6$ the lattice adopts the crystal structure of bulk Sm with the moments forming a six-layer c -axis antiferromagnet. At Ho concentrations $x < 0.4$ the alloys are double hexagonal-close-packed and remain nonmagnetic down to the lowest temperatures studied. Using x-ray magnetic resonance scattering techniques, we demonstrate that a small, static spin-density wave is induced within the alloy $5d$ band at both the Pr and Ho sites in both of the magnetically ordered phases. The interpretation of the data is, however, complicated by the fact that the intensity branching ratio $L_{\text{III}}/L_{\text{II}}$ differs from order unity for both Ho and Pr, in contrast to what is predicted from the simplest models of the resonance process. This suggests that an improved treatment of the full exchange interaction between the $5d$ and $4f$ moments, such as recently proposed by van Veenendaal, Goedkoop, and Thole [Phys. Rev. Lett. **78**, 1162 (1997)], may be needed before quantitative estimates of the magnitudes of the induced $5d$ moments can be obtained. The temperature dependences of the lattice and magnetic structures, including the lattice constants, magnetic wave vectors, magnetic order parameters, and c -axis coherence lengths, are also characterized. [S0163-1829(98)06009-3]

I. INTRODUCTION

In this paper, we report a high-resolution x-ray-scattering study of the magnetic structure and phase behavior of a series of $\text{Ho}_x\text{Pr}_{1-x}$ thin-film alloys, taking particular advantage of the species-sensitivity introduced by x-ray resonant scattering techniques. The present work is a companion to neutron-scattering experiments performed on the same samples and described in the preceding paper,¹ hereafter referred to as paper I. Together these papers elucidate the magnetic properties of the Ho-Pr alloys as well as show how x-ray and neutron-scattering techniques may overlap and complement each other in the study of rare-earth magnetic structures.

The basic interactions underlying rare earth magnetism are well understood.² They include a Ruderman-Kittel-Kasuya-Yosida exchange interaction coupling localized $4f$ moments in competition with crystal-field and magnetoelastic interactions. Long-period, modulated magnetic structures, comprised of a large $4f$ component (typically $5-10 \mu_B/\text{atom}$) and a small, static spin-density wave ($\sim 0.3 \mu_B/\text{atom}$) that is induced in the $5d$ band, are characteristic features. Detailed theoretical accounts of the magnetic structures exhibited by the bulk rare-earth elements have been given using mean-field theory.² Much recent research has been concerned with characterizing the magnetic properties of molecular-beam-epitaxy-grown thin films, including pure metals, alloys, and multilayers.³ In addition to

the fundamental interest in systematically probing the interactions, these studies offer the hope that thin-film magnetic properties might also be controlled. A key issue confronting all such studies remains understanding how the strain introduced at the film/substrate interfaces alters the film magnetic structures.⁴⁻⁶

The materials of interest in this paper are Ho-Pr alloys. In the pure metal, holmium has a hexagonal-close-packed (hcp) chemical lattice and a basal-plane spiral magnetic structure below $T_N \sim 131.5$ K. Its magnetic structure has been well characterized in many neutron- and x-ray-scattering experiments,^{2,7,8} including the separate observations of the $4f$ and induced $5d$ magnetization densities mentioned above.⁹ In contrast, Pr has a double hexagonal-close-packed (dhcp) chemical lattice and the corresponding crystal-field interaction leads to a nonmagnetic singlet ground state. Bulk Pr does not exhibit magnetic ordering until 0.05 K unless subjected to perturbations, such as external pressure or magnetic field.² (References to earlier work on alloys formed from combinations of light and heavy rare-earth elements are given in paper I.)

Our aim in these experiments was first to characterize the lattice and magnetic structures as a function of increasing Pr concentration. Briefly, we have found that our results agree with the main features of the magnetic phase diagram determined by neutron scattering,¹ specifically that the alloys exhibit three distinct phases versus Pr concentration. In the Pr-rich phase (Pr concentration greater than 60%), the chemical lattice has dhcp symmetry and remains nonmagnetic down to 10 K. For Pr concentrations between 40% and 60%, the chemical lattice changes and possesses the structure of bulk Sm. These alloys are magnetic, exhibiting a six-layer antiferromagnet, similar to that found in bulk Sm, and with magnetic ordering temperatures T_N varying between ~ 30 and 60 K, depending on concentration. In the Ho-rich phase (Pr concentration less than 40%) the chemical lattice is hcp and the magnetic structure is a basal-plane spiral, as occurs in bulk Ho. The Néel temperatures fall between ~ 60 and 130 K, again depending on concentration.

For the alloys exhibiting magnetic order, it was also of interest to determine whether the Pr sites support a net magnetization density, either within their $4f$ shells (which would imply a change in the balance between the crystal field and exchange interactions relative to bulk Pr) or induced within the $5d$ bands by the Ho $4f$ moments, or both. An induced $5d$ moment has been observed recently for nonmagnetic Lu atoms when they are dispersed in a magnetic Dy host lattice.¹⁰ By tuning the incident x-ray energy to the L_{III} and L_{II} absorption edges of Ho and Pr, respectively, we have measured the magnetic scattering from the Ho and Pr sites separately. It was found that for both the spiral and Sm magnetic structures there is a static spin density wave induced in the alloy $5d$ bands, which propagates on both the Ho and Pr sites analogous to that in the Dy-Lu alloys. To within the available statistics, the induced Pr $5d$ moment per atom is independent of concentration.

One of the most intriguing results of the present study concerns the branching ratios measured at the L_{III} and L_{II} absorption edges of both Ho and Pr in the 50-50 alloy (Sm magnetic structure). In the simplest theories of the cross section,¹¹ the resonant magnetic intensity determined at a

rare-earth L_{III} edge should approximately equal that obtained at the corresponding L_{II} edge. However, it has recently become clear that L_{III}/L_{II} branching ratios are much greater than 1 for the heavy rare-earth elements while the reverse is true for the lighter elements.^{12,13} We find that this correspondence is preserved in Ho-Pr alloys, which are comprised of both heavy and light constituents, independent of concentration. Resolving this discrepancy with the theory will be required before the induced moment amplitudes can be reliably extracted from the resonant magnetic intensities and is a crucial step for the development of resonant techniques. Moreover, it implies that the simple picture of rare-earth electronic structure employed in these calculations is not adequate. Recent progress has been made in the theory of these processes by van Veenendaal, Goedkoop, and Thole.¹⁴

Finally, we have characterized the temperature dependence of the lattice and magnetic structures, including the magnetic wave vectors, lattice constants, order parameters, and coherence lengths. All of these measurements have benefited from the high wave-vector resolution routinely achievable with x rays. We have found that the temperature dependences of the induced Ho and Pr $5d$ magnetic wave vectors are identical throughout the magnetically ordered phases and are consistent with that of the total moment determined by neutron scattering. Specifically, in the Sm magnetic phase, the magnetic wave vectors remain locked to $\tau = \frac{1}{3}$ for all temperatures, as in bulk Sm. In the spiral magnetic phase the wave vectors decrease continuously from T_N and lock to $\tau \sim \frac{2}{5}$ below ~ 60 K. The temperature dependence of most of the Ho and Pr magnetic order parameters exhibits a power-law dependence near T_N with mean-field exponents, as has been observed previously in other Ho films,¹⁵⁻¹⁷ although not in all of them.^{4,18}

The remainder of this paper is arranged as follows. In Sec. II we discuss the experiment in terms of the crystal structure (Sec. II A), the magnetic structure (Sec. II B), the temperature dependence of the magnetic wave vectors, lattice constants and coherence lengths (Sec. II C), the temperature dependence of the magnetic order parameter (Sec. II D) and the induced Pr moments (Sec. II E). In Sec. III we summarize and give conclusions.

II. EXPERIMENT

The growth of the thin-film $\text{Ho}_x\text{Pr}_{1-x}$ alloy samples is described in paper I. Here it will suffice to say that samples with nominal compositions of $x = 1, 0, 0.8, 0.6, 0.4$ were studied using x-ray-scattering techniques. The x-ray-diffraction experiments were performed mainly on the bending magnet beam line X22C at the National Synchrotron Light Source, with additional measurements performed on BW2 at HASYLAB. NLS X22C is equipped with a doubly focusing nickel-coated mirror and a fixed exit Ge(111) double-crystal monochromator. The samples were mounted in a closed-cycle refrigerator with their $[00L]$ faces oriented in the vertical scattering plane.

High- Q -resolution studies were performed using a Ge(111) analyzer crystal, resulting in a momentum-transfer resolution [full width at half maximum (FWHM)] of 7×10^{-4} , 3.6×10^{-4} , and $2 \times 10^{-2} \text{ \AA}^{-1}$ in the longitudinal, transverse, and out-of-plane directions, respectively. The

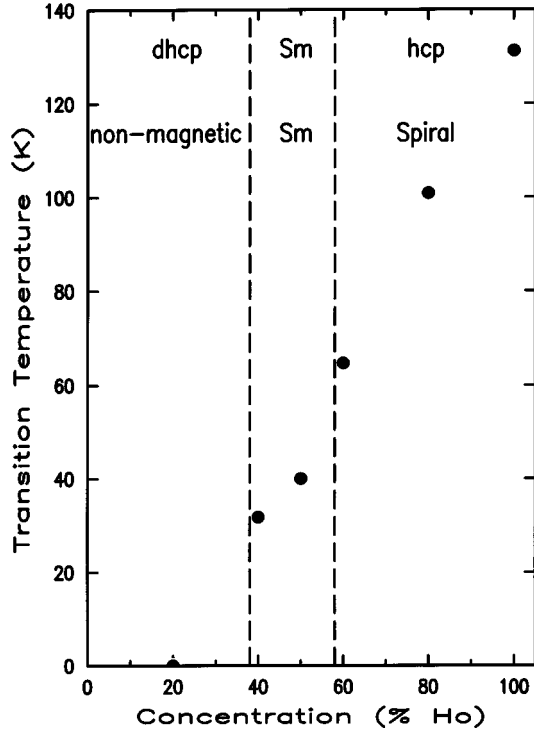


FIG. 1. Phase diagram of the crystal and magnetic structures of the alloys studied. The Néel temperature is reported as a function of Ho concentration.

resolution function was determined approximately from the (1120) reflection of the sapphire substrate. The incident radiation from the bending magnet is $\sim 95\%$ linearly polarized in the plane of the storage ring (σ polarized). In some experiments, the scattered radiation was analyzed using a polarization analyzer mounted on the 2θ arm of the diffractometer. The orientation of polarization analyzer crystal was chosen to select the π component of the magnetic scattering, that is, the component rotated by 90° with respect to the incident polarization or perpendicular to the plane of the storage ring. Graphite(006) and Cu(220) crystals were used as polarization analyzer crystals at the L_{III} (Ho) and L_{II} (Pr) edges respectively.

X-ray resonant magnetic scattering is an element-specific technique that exploits the anomalous cross section for x-ray scattering at an absorption edge. It has been found that large enhancements of the magnetic scattering are observed when the incident photon energy is tuned near an L_{III} or L_{II} absorption edge of a rare-earth metal. The resonant contributions to the cross section may be described on the basis of electric-dipole and quadrupole transitions between $2p$ core states and unoccupied $5d$ and $4f$ valence levels, respectively.^{9,11} Electric-dipole transitions, coupling $2p_{3/2}$ and $5d_{1/2}$ states at the L_{III} edges and $2p_{1/2}$ and $5d_{3/2}$ states at the L_{II} edges, sufficiently dominate the quadrupole transition in the rare-earth elements^{9,12} that we neglect quadrupole transitions in this paper. For a system where the magnetic and charge unit cells have a different periodicity, the electric-dipole contribution to the resonant scattering amplitude at the primary magnetic wave vector is¹¹

$$f_j^E \propto iP(\mathbf{e}_i \times \mathbf{e}_f^*) \cdot \hat{\mathbf{z}}_j, \quad (1)$$

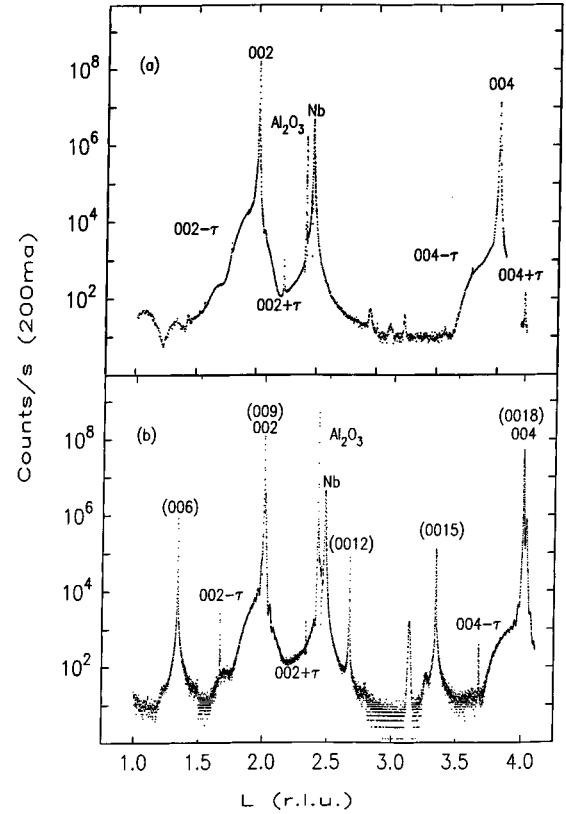


FIG. 2. Longitudinal scan along $[00L]$. (a) $\text{Ho}_{0.6}\text{Pr}_{0.4}$ alloy. Spiral magnetic structure and hcp crystal structure. (b) $\text{Ho}_{0.5}\text{Pr}_{0.5}$ alloy. Sm magnetic structure and Sm crystal structure.

where \mathbf{e}_i and \mathbf{e}_f are the incident and the scattered polarization unit vectors and \mathbf{z}_j is the unit vector parallel to the magnetic moment on the j th atom. The factor P includes various contributions and may be approximated as

$$P \approx \frac{r_0}{x-i} \left(-n_u + \delta n_h + \frac{\Delta}{\Gamma(x-i)} n_h \right), \quad (2)$$

where x is a measure of the energy offset from resonance in units of the half-width of the resonance $\Gamma/2$. The other factors in Eq. (2) depend on properties of the $5d$ bands: n_u is the net spin polarization, n_h is the number of holes per atom, δ is the difference in matrix elements for the spin-up and spin-down bands, and Δ is the exchange splitting. Thus the resonant dipole intensity reflects the magnetization density induced within the $5d$ bands by the localized $4f$ moment. At an L -edge resonance of one of the constituents of a rare-earth alloy, the positions and intensities of the dipole scattering reflect the site-specific $5d$ magnetization density, as has been demonstrated earlier in Ho-Er,¹⁹ Ho-Tb,²⁰ and Dy-Lu alloys.¹⁰ This is the key fact underlying the experiments described in this paper. However, it is important to note that extracting the magnitude of the moment from the intensities remains a challenge, as will be discussed in detail in Sec. II E on rare-earth branching ratios. From Eq. (1) it is seen that for linearly σ -polarized incident x rays, in the dipole approximation the scattered radiation from a magnetic spiral or from the Sm magnetic structure is π polarized.

A. Crystal structure

The crystal structure of bulk Ho is hcp with stacking sequence *ABAB*, while that of Pr bulk is dhcp with stacking sequence *ABACA*. As established by the neutron-scattering experiments¹ performed on these samples, the chemical structure changes from hcp to the rhombohedral structure of samarium and then to dhcp, by alloying Ho with an increasing concentration of Pr. This is shown in the phase diagram of Fig. 1. The Sm structure^{21,22} is rhombohedral and corresponds to the space group $R\bar{3}m$ (D_{3d}^5). It may be considered as three interpenetrating rhombohedra with three lattice points in the unit cell, whose atomic positions are at (0,0,0) and $\pm(\mu, \mu, \mu)$, where $\mu = \frac{2}{3}$. In transforming from rhombohedral to hexagonal coordinates, the new hexagonal unit cell has nine equidistantly spaced layers, where the stacking sequence is $[ABABCBCAC]AB$. The new nine lattice points are at the following positions: $(0,0,0), (\frac{2}{3}, \frac{1}{3}, \frac{1}{3}), (\frac{1}{3}, \frac{2}{3}, \frac{2}{3})$ and $(0,0, \pm\mu), (\frac{2}{3}, \frac{1}{3}, \frac{1}{3} \pm \mu), (\frac{1}{3}, \frac{2}{3}, \frac{2}{3} \pm \mu)$. Two-thirds of the sites have near-neighbor layer configurations similar to that found in the simple hexagonal structure *ABAB* and one-third are similar to that of the fcc structure *ABCABC*. It is shown in paper I that the Ho atoms preferentially occupy hexagonal sites in the Sm-like alloys. The allowed reflection conditions are $-h+k+l=3n$, $-h+k=3n$, and $h+l=3n$, where n is an integer. For convenience we will mostly use the hcp indices in the following.

Representative scans of the $\text{Ho}_{0.6}\text{Pr}_{0.4}$ (hcp structure) and $\text{Ho}_{0.5}\text{Pr}_{0.5}$ (Sm structure) taken along the $[00L]$ direction at 10 K are shown on a logarithmic scale in Figs. 2(a) and 2(b), respectively. The charge-scattering peaks associated with the chemical lattice of the $\text{Ho}_{0.6}\text{Pr}_{0.4}$ alloy [Fig. 2(a)] are indexed in hcp units. The magnetic peaks are labeled $(0,0,2 \pm \tau)$ and $(0,0,4 \pm \tau)$, where τ is the magnetic wave vector. Peaks originating from the sapphire substrate or Y seed are labeled accordingly. The charge scattering peaks of the $\text{Ho}_{0.5}\text{Pr}_{0.5}$ alloy are indexed in both hcp and Sm units, the latter shown in parentheses. Magnetic peaks are again labeled with reference to the hcp basis (with $\tau = \frac{1}{3}$). The origin of the clusters of peaks appearing near $L=1.3$ and 3.0 in Fig. 2(a) and near $L=3.2$ in Fig. 2(b) is not understood. Their persistence in the diffraction patterns for temperatures above the respective Néel temperatures, however, suggests that they are neither magnetic nor magnetoelastic in origin and we have not studied them further. Although we have not performed detailed intensity analysis of the charge-scattering peaks in the alloy series, we note that the positions and qualitative intensities of the charge scattering peaks are consistent with hcp and Sm structures assigned in the neutron-scattering experiments described in paper I.

Longitudinal scans of the charge and magnetic scattering were fitted to squared-Lorentzian line shapes for all of the samples studied in these experiments. Transverse scans were fitted to Lorentzian line shapes. These line shapes were chosen for convenience of fitting; no significance is attached to their forms. The mosaic spreads, together with the interplanar lattice spacings, and Néel temperatures are reported for each sample in Table I. The mosaics for these samples are all similar, varying between 0.1° and 0.2° . The c -axis coherence lengths for the chemical and magnetic lattices are reported in

TABLE I. Some parameters of the samples studied. The interplanar spacing for the alloys was measured at $T=10$ K.

x	Mosaic spread (deg)	Interplanar spacing (Å)	Néel T (K)
1 ^a	0.22	2.81	131
0.8	0.17	2.823	100.86
0.6	0.13	2.846	64.73
0.5	0.14	2.878	40.01
0.4	0.13	2.882	31.79
0.0 ^b		2.910	106
0.0 ^c		2.958	0.05

^aHo film.

^bBulk Sm at $T=300$ K.

^cBulk Pr at $T=300$ K.

Table II. Except for the $\text{Ho}_{0.6}\text{Pr}_{0.4}$ film, the average c -axis lattice coherence lengths fall between 1200 and 1700 Å, which is typical of the best rare-earth films grown to date. It should be noted that the structural coherence lengths reported in paper I were deduced from $(10L)$ scans, not $(00L)$ scans as reported here, and are therefore sensitive to the *ABA...* stacking sequences in the films. Those lengths were observed to be shorter than the pure c -axis coherence lengths, which mainly reflect the interplanar spacing along the c axis. The variation of the observed Néel temperatures with concentration is also discussed in detail in paper I.

B. Magnetic structure

The magnetic structures of the sequence of Ho-Pr alloys were studied by scanning the momentum transfer along the $[00L]$ and $[10L]$ directions, both as a function of temperature and as a function of incident photon energy. Representative scans along the $[00L]$ direction obtained at the Ho L_{III} edge at $T=10$ K are shown in Fig. 2 for the two different magnetic phases observed in this work. The magnetic peaks are all indexed in hcp units with the magnetic wave vectors referred to the $(0,0,2)$ and $(0,0,4)$ reflections. In all such scans, whether along the $[00L]$ or $[10L]$ direction, the positions of the magnetic peaks were found to be consistent with the symmetries assigned in the neutron-scattering studies of these alloys and reported in paper I. Specifically, the x-ray-scattering results are consistent with a spiral magnetic structure in the hcp phase (corresponding to $x=0.8$ and 0.6) and with a Sm magnetic structure in the Sm phase (corresponding to $x=0.5$ and 0.4). In the spiral magnetic phase, which

TABLE II. Coherence length of the chemical and magnetic lattices.

x	FWHM (002) (Å ⁻¹)	Coherence length (002) (Å)	FWHM (002- τ) (Å ⁻¹)	Coherence length (002- τ) (Å)
1 ^a	0.001 68	1200	0.0022	900
0.8	0.001 25	1600	0.0021	1000
0.6	0.0028	700	0.003	700
0.5	0.0012	1700	0.0012	1700
0.4	0.0017	1200	0.003	700

^aHo film.

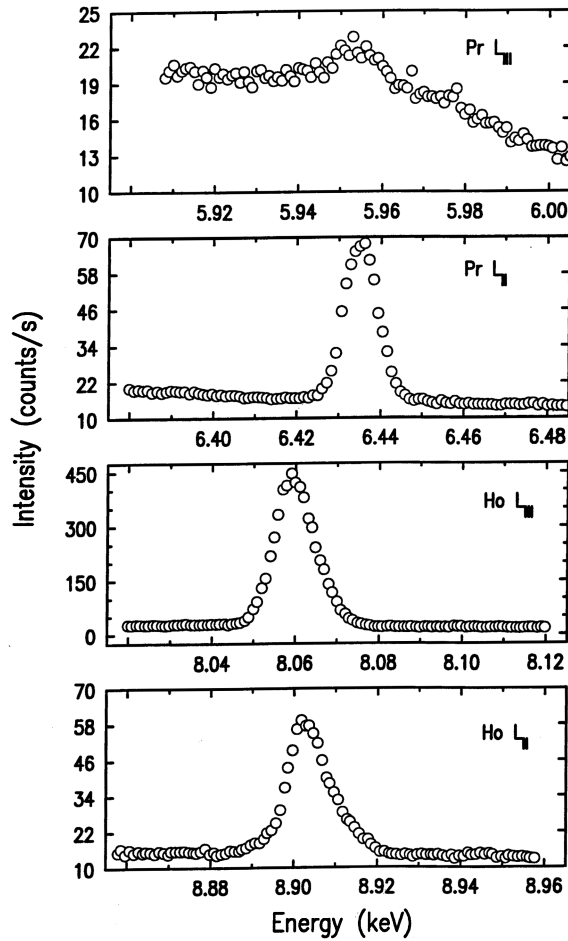


FIG. 3. Energy scans of the magnetic peak ($002-\tau$) collected at the Ho L_{III} and L_{II} and Pr L_{III} and L_{II} absorption edges of the $\text{Ho}_{0.5}\text{Pr}_{0.5}$ alloy.

characterizes bulk holmium, the atomic moments are ferromagnetically aligned within the basal planes, but rotate from plane to plane with a temperature-dependent turn angle $\phi = \tau\pi$. The magnetic structure of bulk Sm is a six-layer c -axis antiferromagnet described by a wave vector $\tau = \frac{1}{3}c^*$ (see paper I for more details).

The full widths of the magnetic reflections were found to be comparable to those from the chemical lattice, falling between 0.0012 and 0.003 \AA^{-1} as measured at the $(0,0,2-\tau)$ reflections (see Table II). These correspond to c -axis magnetic coherence lengths between 700 and 1700 \AA along the c axis, which is again typical of most rare-earth thin films studied to date. As noted earlier, no magnetic scattering was observed in the dhcp phase ($x < 0.4$) by x-ray or neutron scattering, down to 23 mK .

The energy dependence of the magnetic scattering of the $\text{Ho}_{0.5}\text{Pr}_{0.5}$ alloy at the $(0,0,2-\tau)$ reflection is shown in Fig. 3, as the incident photon energy was tuned through each of the Ho and Pr L_{II} and L_{III} edges. These data were obtained at $T = 10 \text{ K}$ using a Ge(111) analyzer crystal. The strongest enhancements were found at the Ho L_{III} and Pr L_{II} edges across the alloy series, as is clear in Fig. 3 for the $\text{Ho}_{0.5}\text{Pr}_{0.5}$ sample. The resonant full widths ($\sim 10 \text{ eV}$) reflect the atomic widths of the L excitations (typically $5\text{--}10 \text{ eV}$) convolved with the

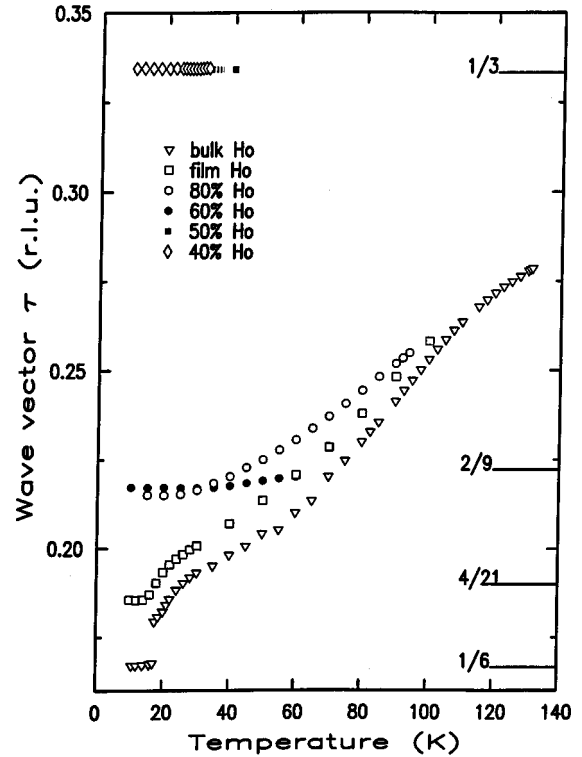


FIG. 4. Temperature dependence of the magnetic wave vector for four alloy films, a bulk Ho sample, and a pure Ho thin film. The data shown were collected at the Ho L_{III} edge. The temperature dependence of the magnetic wave vector was also measured at the Pr L_{II} absorption edge for the four alloys and resulted in exactly the same behavior as shown.

energy resolution of the beam line ($\leq 10 \text{ eV}$). As discussed in more detail below, the existence of dipole resonant scattering at the Pr and Ho L edges implies that there is an induced magnetization density within the alloy $5d$ band, which is present at both Pr and Ho sites. The symmetry of the magnetic diffraction patterns shown in Fig. 2 for the spiral and Sm magnetic structures was preserved at resonance independently of whether the incident photon energy was tuned to a Ho or Pr edge. This suggests that the magnetic structure of the spin-density wave is consistent with that determined for the total moment by neutron scattering.

C. Temperature dependence of the magnetic wave vectors, lattice constants, and coherence lengths

In Fig. 4 we summarize the temperature dependence of the magnetic wave vectors for the different magnetically ordered alloys, after correction for the temperature variation of the c -axis lattice constants. Identical results were obtained at both the Ho L_{III} and Pr L_{II} resonances in each sample, consistent with the results of neutron scattering. In the simple spiral phase of the $x = 0.80$ sample, the magnetic wave vector decreases continuously from about $\tau = 0.25$ at $T = T_N = 110 \text{ K}$ until about $T = 30 \text{ K}$, where it locks into a value $\tau = 0.215 \pm 0.002$. The behavior of the other Ho-rich alloy ($x = 0.60$) is qualitatively similar, although the decrease in wave vector occurs over a much narrower temperature range,

from about $T=T_N=60$ K to $T=30$ K and locks into $\tau=0.217\pm 0.002$. Both alloys exhibiting the Sm magnetic structure have wave vectors locked into $\tau=\frac{1}{3}$ throughout their ordered phases, consistent with bulk Sm.

The temperature dependence of the magnetic wave vectors in the holmium-rich samples is qualitatively similar to that observed in bulk and thin-film Ho, as shown by the open triangles and squares in Fig. 4, respectively. In the bulk, the magnetic wave vector decreases continuously from about $\tau=0.28$ at $T=T_N=131.5$ K until about $T=20$ K, where it locks into $\tau=\frac{1}{6}$, whereas the thin-film wave vector locks into $\tau=\frac{4}{21}$. The $\frac{1}{6}$ phase of Ho is well understood² and corresponds to a conical magnetic spiral with a ferromagnetic component along the c axis. The in-plane structure is a bunched spiral, in which the moments on pairs of adjacent planes are slightly distorted toward the six easy directions of the hexagonal basal planes. The $\frac{4}{21}$ structure is a simple spin-slip structure⁸ that may be formed from the $\frac{1}{6}$ structure by replacing every fourth pair of planes in the spiral by a single plane, i.e., (1222)(1222)(1222). Here a 1 represents a single plane or spin slip and a 2 represents a pair of planes. The nearness of the observed lock-in wave vectors in the $x=0.8$ and 0.6 samples to $\tau=\frac{2}{9}\sim 0.22$ suggests a spin-slip description in this case as well (12)(12)(12), with a spin-slip occurring for every pair of planes. The occurrence of lock-in transformations to spin-slip structures reflects the large six-fold crystal-field anisotropy of holmium at low temperatures and the clamping of the film by its substrate.

The temperature dependences of the average c -axis lattice constants and inverse magnetic coherence lengths are shown in Figs. 5(a) and 5(b), respectively. Referring first to the c -axis lattice constants, it is seen that their low-temperature values increase with increasing Pr concentration and approach the interplanar spacing of bulk Sm (5.82 Å on this scale) for Sm-like $\text{Ho}_{0.5}\text{Pr}_{0.5}$ and $\text{Ho}_{0.4}\text{Pr}_{0.6}$ samples. (The interplanar layer spacings are compared directly in Table I.) There is little temperature variation of any of the lattice constants on the scale of Fig. 5(a). The greatest change occurs for the $\text{Ho}_{0.8}\text{Pr}_{0.2}$ sample, which is shown on a finer scale in the inset (dotted line). The observed increase below T_N is consistent with that recorded in a pure holmium film (open squares) and is due to magnetostriction. However, it is clear that the absolute values of the alloy lattice constants are expanded relative to pure holmium by between 0.3% for the $x=0.8$ sample and 3% for the $x=0.4$ sample. The largest expansion corresponds to the samples in the intermediate-concentration regime that exhibit the Sm crystal structure. The a -axis values are clamped by the substrate and do not vary with temperature.

The longitudinal full widths of the magnetic scattering [Fig. 5(b)] are also approximately independent of temperature, except near their respective magnetic ordering temperatures, where they increase (corresponding to a decrease in the magnetic coherence length). The small increase in width also observed in the $x=0.8$ sample near $T=30$ K probably reflects the approach of the conical transition at low temperatures and has been observed previously in thin Ho films.¹⁸ It is interesting that the average c -axis lattice and magnetic coherence lengths (see Table II for the latter) are shorter for both the $x=0.6$ and 0.4 samples than for the $x=0.8$ and 0.5 samples. These concentrations lie near the boundaries sepa-

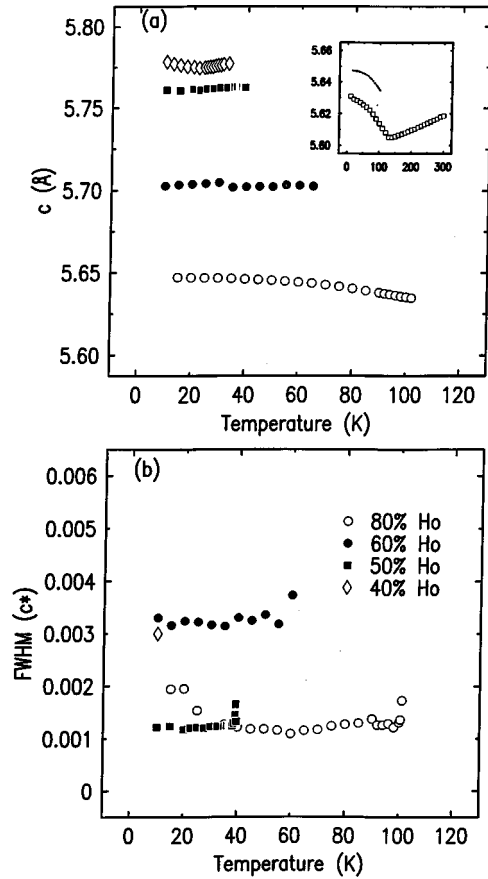


FIG. 5. (a) Temperature dependence of the c -axis lattice parameters. Inset: detail of the $\text{Ho}_{0.8}\text{Pr}_{0.2}$ sample (dotted line) compared to a pure Ho film. (b) Temperature dependence of the full widths at half maximum of the $(002-\tau)$ magnetic peaks. High-resolution scans of the $\text{Ho}_{0.4}\text{Pr}_{0.6}$ sample (open diamond) were made only at $T=10$ K.

rating the hcp Sm and Sm dhcp phases and we speculate that the reduced coherence lengths may reflect a corresponding structural metastability, also noted in paper I.

D. Temperature dependence of the magnetic order parameter

The integrated intensity of the magnetic scattering was measured as a function of temperature at the $(0,0,2-\tau)$ reflection along the longitudinal direction for all four magnetic alloys at the Ho L_{III} ($=8.071$ keV) and Pr L_{II} ($=6.440$ keV) edges. Longitudinal scans offer the simplest means for separating the magnetic scattering from the charge-scattering background due to the film reflectivity. However, transverse scans were also taken at the magnetic peak positions to check for consistency. For alloys of concentration $x=0.6, 0.5, 0.4$, the data were collected using the polarization analyzer set to select the σ to π component of the magnetic scattering. For the $x=0.8$ alloy, a Ge(111) analyzer was used due to the very weak signal at the Pr edge.

A representative plot for the $\text{Ho}_{0.5}\text{Pr}_{0.5}$ sample is shown on a linear scale in Fig. 6(a). The intensities collected at the Pr edge have been multiplied by a constant, for easy comparison with the intensities obtained at Ho edge. It is clear

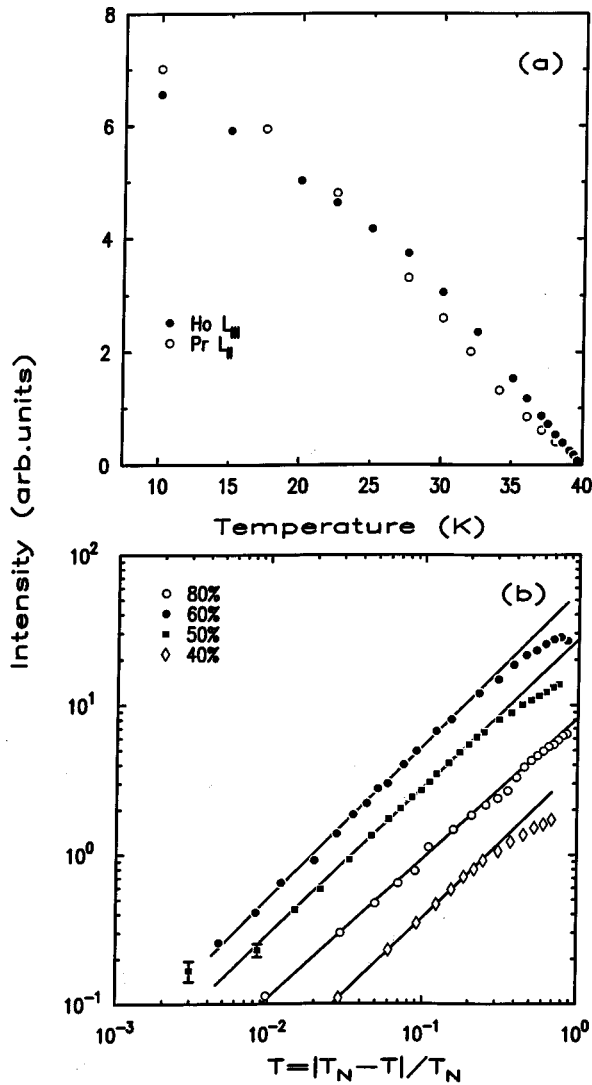


FIG. 6. (a) Order parameters collected at the Ho L_{III} and Pr L_{II} absorption edges for the 50% Ho concentration sample. (b) Order parameters collected at the Ho L_{III} edge for the four thin alloy films. The curves are fitted to a power law in reduced temperature $I \sim (T_N - T)^{2\beta}$; the values of β are reported in Table III.

from the figure that the data for Pr preclude a reliable, quantitative comparison with the Ho, although qualitatively the two data sets are consistent with each other to within estimated errors. Instead, the Ho resonance data were fitted separately to a power law in reduced temperature $I \sim (T_N - T)^{2\beta}$ [see Fig. 6(b)] and the values of β were extracted for all the alloys. The fitted values of the order parameter β are shown in Table III and were determined by analyzing the

TABLE III. Fitted values of the order parameter β and T_N as function of Ho concentration.

x	T_N	β
40	31.79 ± 0.1	0.49 ± 0.05
50	40.01 ± 0.1	0.5 ± 0.05
60	64.73 ± 0.1	0.56 ± 0.05
80	100.86 ± 0.1	0.42 ± 0.05

data within about $(T - T_N)/T_N \sim 20\%$. Most of these values fall near $\frac{1}{2}$, in agreement with the results obtained by neutron scattering on the $x=0.6$ sample¹ and on several pure Ho films.^{16,15,17} It is interesting that β appears smaller than $\frac{1}{2}$ for the $x=0.8$ sample, in agreement with bulk measurements, which cluster around 0.39, and with at least one other pure Ho film.^{4,18}

E. Induced Pr moment

One of the unique features of the cross section for resonant x-ray magnetic scattering is its selectivity in studying the magnetic ordering of different atomic species, which is accomplished by tuning the incident x-ray energy to an L or M absorption edge of the chosen atom. Indeed, the selection rules governing the electric-dipole and -quadrupole scattering permit identification not only of the species, but also of the symmetry of the magnetic states, for example, whether a magnetic moment resides within a $5d$ or $4f$ orbital or both.⁹ A main objective of the experiments described in this section was to use these techniques to determine whether a small magnetic moment is induced on the Pr atoms within the alloy $5d$ bands and then to estimate its magnitude with respect to that induced on the Ho atoms, as a function of increasing Pr concentration. Related experiments have shown recently that in Dy-Lu alloys a small $\sim 0.2\mu_B$ moment is induced within alloy $5d$ bands on the Lu atoms by the Dy $4f$ moments. The latter results are interesting since atomic Lu has a filled $4f$ shell and is nonmagnetic in the metallic state. In contrast, atomic Pr has two electrons in its $4f$ shell and a nonmagnetic singlet ground state in its metallic state, which does not exhibit magnetic ordering until $T_N = 0.05$ K. However, the degeneracy of the ground state is lifted in the presence of an applied pressure or magnetic field.² It is also interesting to ask whether the change in the lattice symmetry for alloys with $0.4 < x < 0.6$ is sufficient to alter the Pr ground state leading to a Pr $4f$ moment.

A second motivation for these experiments was to explore the dependence of the measured L_{II}/L_{III} “branching ratios” in the rare-earth elements on their $4f$ occupancy. More specifically, it has been found in both x-ray resonant magnetic scattering and x-ray magnetic circular dichroism experiments that the magnetic intensities obtained at the L_{III} edges of the heavier rare-earth elements (Tb and higher) are ~ 10 times stronger than those obtained at the corresponding L_{II} absorption edges. In contrast, the intensities obtained at the L_{II} edges of the lighter rare-earth elements (Sm and lower) are stronger than obtained at the L_{III} edges.^{12,13} This is surprising because the existing theories of resonant magnetic scattering and absorption predict that the branching ratios should be near unity across the series. From this perspective, the $\text{Ho}_{0.5}\text{Pr}_{0.5}$ random alloy is an ideal test system, as it combines both light and heavy rare-earth elements in the same lattice and permits the Ho and Pr branching ratios to be determined under identical experimental conditions.

Integrated intensities were obtained at both the $(002 - \tau)$ magnetic and (002) Bragg reflections for each of the Ho and Pr L_{II} and L_{III} absorption edges and for each magnetic alloy. The measurements were performed using a Ge(111) analyzer crystal and involved scanning the reflections in both the longitudinal and transverse directions. Scans of the (002) Bragg

TABLE IV. Normalized intensity ratio $(002-\tau)/(002)$ (10^{-7}). An asterisk denotes cases in which scattering was too weak to permit integrated intensities to be calculated.

Absorption edge \ Ho concentration (%)	80	60	50	40
Pr L_{III}	*	*	0.52 ± 0.063	*
Pr L_{II}	1.54 ± 0.22	4.2 ± 0.27	5.79 ± 0.3	6.95 ± 0.3
Ho L_{III}	110 ± 8	48.0 ± 1.2	43.5 ± 3.0	17.1 ± 0.5
Ho L_{II}	*	4.02 ± 0.2	4.78 ± 0.2	1.96 ± 0.2

reflections, at the four absorption energies, required the use of calibrated Al absorbers in order that the charge and magnetic scattering could be directly compared. In the fits, it was found that the respective longitudinal and transverse widths were all approximately equal, independent of concentration, allowing the integrated intensities to be calculated from scans in either direction. Longitudinal scans were chosen for this purpose as the specular reflectivity from the multiple thin-film interfaces introduces a significant, θ -dependent background in the transverse scans, which requires additional corrections. Although the integrated intensities obtained from both kinds of scans were found to be consistent, those obtained from longitudinal scans are believed to be the more reliable.

The ratios of the integrated magnetic ($002-\tau$) and charge (002) intensities obtained for each of the Ho and Pr L_{II} and L_{III} absorption edges and for each magnetic alloy are shown in Table IV. By dividing the magnetic satellite intensities by the intensities of the nearby charge-scattering peaks at each energy, we approximately correct for the dependence of the incident x-ray intensity on energy and for the absorption.²³ Resonant magnetic scattering was observed at the Ho L_{III} and Pr L_{II} absorption edges in all the alloys. However, in most cases the scattering at the Pr L_{III} edge was too weak to permit integrated intensities to be calculated. These are indicated by an asterisk in Table IV.

From the existence of resonant scattering at each of the Pr L_{II} edges in the alloys, we can infer the existence of an induced Pr moment in all of the magnetic samples, as already noted. Polarization analysis of the Pr scattering has shown further that (to within our statistics) it corresponds mainly to the σ -to- π channel, which implies for both the spiral and Sm structures that there exists an induced moment on the Pr atoms within the $5d$ bands, consistent with dipole selection rules. (Dipole resonant behavior was also observed, of course, at each of the Ho L_{II} edges). It is reasonable to conclude, therefore, that the static spin-density wave induced within the alloy $5d$ band by the Ho $4f$ moments propagates at both Ho and Pr sites. In the present experiments we have not been able to establish directly whether there is also an induced $4f$ moment at the Pr sites (for example, by detecting resonant quadrupole scattering at a Pr L absorption edge). However, on the basis of an analysis of the neutron magnetic scattering intensities, it is concluded in paper I that the full Pr $4f$ moment develops in each magnetic alloy.¹

The integrated intensities of the $(002-\tau)$ magnetic peaks obtained at the Pr L_{II} edge, divided by their respective (002) charge intensities and normalized by concentration, are shown plotted versus Pr concentration in Fig. 7. This quantity corresponds to the resonant Pr intensity per atom, which

the simplest theories¹¹ predict is approximately proportional to the modulus squared of the induced $5d$ moment per atom. From the plot it appears that the induced moment on each Pr atom is the same in all the alloys to within the error bars.

We attempted to estimate the magnitudes of the induced Pr $5d$ moments using the same techniques employed by Everitt *et al.* on Dy-Lu alloys. In their work, the induced Lu $5d$ moment was obtained by taking the ratio of the Ho and Lu L_{III} intensities, after corrections for absorption, exchange splitting, radial matrix elements, concentration, etc. The intensity ratio was then approximated as

$$P_{Lu} = \frac{\langle r \rangle_{Dy}^2}{\langle r \rangle_{Lu}^2} \sqrt{\frac{C_{Dy} \mu_{Dy} I_{Lu}}{C_{Lu} \mu_{Lu} I_{Dy}}} P_{Dy}^2,$$

where I corresponds to the integrated intensity of each element, C to the concentration, μ to the absorption coefficient, $\langle r \rangle$ to species-specific radial matrix elements, and P to the spin-polarization factor defined earlier. Suitable estimates of these quantities were made for Dy and Lu and the induced moment on the Lu atoms within the $5d$ band were thereby deduced in terms of the induced moment at the Dy sites.

Similar arguments have been made in the present case, interpolating between the radial matrix elements of Ce and Nd in order to obtain values for Pr.²⁴ Specifically, we used, for Ho L_{II} , $\langle 2p_{1/2} | r | 5d \rangle = 0.0043$, for Ho L_{III} , $\langle 2p_{3/2} | r | 5d \rangle = 0.00472$, for Pr L_{II} , $\langle 2p_{1/2} | r | 5d \rangle = 0.0059$, and for Pr L_{III} , $\langle 2p_{3/2} | r | 5d \rangle = 0.00630$. Assuming for sim-

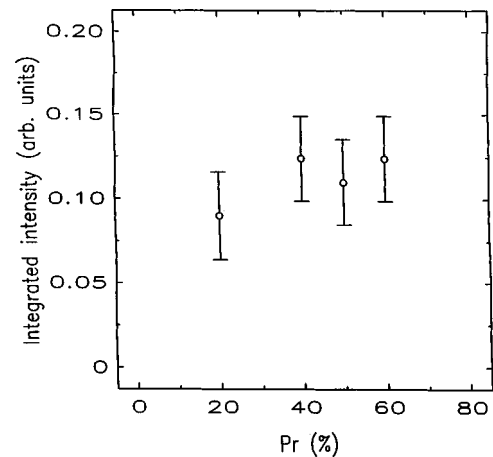


FIG. 7. Integrated intensity of the $(002-\tau)$ magnetic peak at the Pr L_{II} edge in the four alloys studied. The data are normalized to the integrated intensity of the nearby (002) Bragg peak in each case and corrected for concentration.

plicity that there is no self-moment from the Pr $4f$ moments, the ratio of the Ho and Pr L_{III} intensities then gives $P_{Pr} \sim 0.061P_{Ho}$ for the $Ho_{0.5}Pr_{0.5}$ sample. If the induced moment within the Ho $5d$ band is about $0.3\mu_B$, this implies an induced moment within the Pr of about $0.018\mu_B$. It is clear from Table IV, however, that if the same arguments are applied using the intensities obtained at the Ho and Pr L_{II} absorption edges, then $P_{Pr} \sim 0.58P_{Ho}$, which leads to an induced moment on the Pr of about $0.17\mu_B$. This discrepancy reflects the branching ratio problem, which must be overcome before quantitative estimates can be made of the induced Pr moments. These effects are probably less pronounced in Dy-Lu alloys since both Dy and Lu have greater than half-filled $4f$ shells. However, the L_{II} edge intensities of Lu were not obtained in the work of Everitt *et al.*,¹⁰ so that a measure of the size of these effects in that case is not available.

The Ho and Pr branching ratios are easily obtained from Table IV. After correction for the concentration, the Ho L_{II}/L_{III} branching ratio was measured in three of the four alloys and is ~ 0.1 . The Pr L_{II}/L_{III} ratio was measured only in the $x=0.5$ alloy and is ~ 10 . These values correspond to the values found earlier for bulk Ho and Nd (Refs. 9, 12, and 13) and are consistent with the branching ratios found in rare-earth elements by magnetic circular dichroism. They are clearly different from the predictions that give near unity branching ratios. However, they are qualitatively consistent with the recent calculations of the magnetic cross section of van Veenendaal, Goedkoop, and Thole,¹⁴ who extended an earlier analysis to include the coupling of the $5d$ electrons to the $4f$ shell in the excited state. They found that the $5d$ orbitals may be attracted to the $4f$ shell when their spins are parallel ("breathing"), which introduces important corrections. The additional terms depend on the spin state of the excited $5d$ orbitals (whether $d_{3/2}$ or $d_{5/2}$) and on the filling of the $4f$ orbitals across the series and give the qualitative features observed. A more quantitative comparison with our data, including extraction of the induced moment magnitudes, will require further developments of the theory.

Finally, it is worth noting that we have also measured the intensities obtained at the $(002-\tau)$ reflection upon integration over the incident photon energy (see Fig. 3). After nor-

malization by the (002) charge-scattering measured at resonance, it is found that the so-obtained branching ratios mirror those shown in the preceding paragraph.

III. SUMMARY

We have reported a detailed x-ray resonant scattering study of the structural and magnetic phase behavior of a series of Ho_xPr_{1-x} thin-film alloys with holmium composition in the range $40\% < Ho < 80\%$. The observed magnetic structures are Sm-like for $40\% < Ho < 60\%$ and spirals for $Ho > 60\%$. The change in the magnetic structure is accompanied by a change in the chemical lattice from Sm-like to hcp. Each of the magnetic alloys exhibited a concentration-dependent Néel temperature and simply commensurate wave vectors at low temperatures. In the Sm-like phase, the magnetic wave vectors remain locked into $\tau_m = \frac{1}{3}$ at all temperatures, while in the spiral phase they lock into a value near $\tau_m = \frac{2}{9}$. X-ray resonant magnetic scattering techniques were used to show that a small static spin-density wave is induced in the alloy $5d$ bands, propagating at both the Ho and Pr sites of the spiral and Sm-like magnetic structures. To within the available statistics, it was found that the induced Pr $5d$ moment per atom was independent of concentration. Among the most intriguing results of these studies was the observation of anomalous L_{III}/L_{II} branching ratios for Ho and Pr, just as previously observed in pure elements. Specifically, it was found that L_{III}/L_{II} (Ho) ~ 10 and L_{III}/L_{II} (Pr) ~ 0.1 . These results differ from the near-unity branching ratios predicted by the simplest theories. However, they are qualitatively consistent with recent calculations of van Veenendaal, Goedkoop, and Thole,¹⁴ who consider the coupling of the excited $5d$ orbitals to the $4f$ shell. It remains to make quantitative connections between our results and their theory.

ACKNOWLEDGMENTS

It is a pleasure to acknowledge helpful conversations with Michel Veenendaal and Roger Cowley. This work was supported by the National Science Foundation, Grant No. HRD9627065, and by U.S. Department of Energy, Division of Materials Sciences, Contract No. DE-AC02-76CH00016. G.H. acknowledges the support of the Research Council of Norway.

¹J. P. Goff, C. Bryn-Jacobsen, D. F. McMorro, G. J. McIntyre, J. A. Simpson, R. C. C. Ward, and M. R. Wells, preceding paper, Phys. Rev. B **57**, 5933 (1998).

²J. Jensen and A. R. Mackintosh, *Rare Earth Magnetism* (Clarendon, Oxford, 1991).

³See, for example, C. F. Majkrzak *et al.*, Adv. Phys. **40**, 99 (1991).

⁴G. Helgesen, J. P. Hill, T. R. Thurston, Doon Gibbs, J. Kwo, and M. Hong, Phys. Rev. B **50**, 2990 (1994).

⁵M. J. Conover, A. Kaldowsky, and C. P. Flynn, Phys. Rev. B **53**, R2938 (1996).

⁶R. A. Cowley, D. F. McMorro, P. P. Swaddling, R. C. C. Ward, and M. R. Wells, Ind. J. Pure Appl. Phys. **33**, 509 (1995).

⁷R. A. Cowley and S. Bates, J. Phys. C **21**, 4113 (1988).

⁸Doon Gibbs, D. E. Moncton, K. L. D'Amico, J. Bohr, and B. H. Grier, Phys. Rev. Lett. **55**, 234 (1985); J. Bohr, Doon Gibbs, D. E. Moncton, and K. L. D'Amico, Physica A **140**, 349 (1986).

⁹Doon Gibbs, D. R. Harshman, E. D. Isaacs, D. B. McWhan, D. Mills, and C. Vettier, Phys. Rev. Lett. **61**, 1241 (1988); Doon Gibbs, G. Grübel, D. R. Harshman, E. D. Isaacs, D. B. McWhan, D. Mills, and C. Vettier, Phys. Rev. B **43**, 5663 (1991).

¹⁰B. A. Everitt, M. B. Salamon, B. J. Park, C. P. Flynn, T. Thurston, and Doon Gibbs, Phys. Rev. Lett. **75**, 3182 (1995).

¹¹J. P. Hannon, G. T. Trammel, M. Blume, and Doon Gibbs, Phys. Rev. Lett. **61**, 1245 (1988).

¹²J. P. Hill, A. Vigliante, Doon Gibbs, J. L. Peng, and R. L. Greene, Phys. Rev. B **52**, 6575 (1995).

¹³D. Watson, E. M. Forgan, W. J. Nuttall, W. G. Stirling, and D. Fort, Phys. Rev. B **53**, 726 (1996).

¹⁴M. van Veenendaal, J. B. Goedkoop, and B. T. Thole, Phys. Rev. Lett. **78**, 1162 (1997).

¹⁵P. M. Gehring, A. Vigliante, D. F. McMorro, Doon Gibbs, C.

- F. Majkrzak, G. Helgesen, R. A. Cowley, R. C. C. Ward, and M. R. Wells, *Physica B* **221**, 398 (1996).
- ¹⁶D. F. Mc Morrow, A. Vigliante, P. P. Swaddling, J. P. Hill, Doon Gibbs, G. Helgesen, R. A. Cowley, R. C. C. Ward, and M. R. Wells (unpublished).
- ¹⁷R. A. Cowley, R. C. C. Ward, M. R. Wells, M. Matsuda, and B. Sternlieb, *J. Phys.: Condens. Matter* **6**, 2985 (1994).
- ¹⁸G. Helgesen, J. P. Hill, T. R. Thurston, and Doon Gibbs, *Phys. Rev. B* **52**, 9446 (1995).
- ¹⁹D. B. Pengra, N. B. Thoft, M. Wulff, R. Feidenhans'l, and J. Bohr, *J. Phys.: Condens. Matter* **6**, 2409 (1994).
- ²⁰A. Stunault, C. Vettier, F. de Bergevin, F. Maier, G. Grubel, R. M. Galera, and S. B. Palmer, *J. Magn. Magn. Mater.* **140-144**, 753 (1995).
- ²¹C. Koehler and R. E. Moon, *Phys. Rev. Lett.* **29**, 1468 (1972).
- ²²F. H. Ellinger and W. H. Zachariasen, *J. Am. Chem. Soc.* **75**, 5650 (1953).
- ²³This approximation assumes that the resonant processes governing the charge scattering intensities at the Ho and Pr L_{II} and L_{III} edges are sufficiently similar that these intensities may be used as a normalization. It is comforting in this regard that the branching ratios obtained by this procedure in the alloy for Ho match those obtained using an absorption correction in bulk (Ref. 9) and it suggests that the ratio obtained here for Pr is reliable.
- ²⁴M. Hamrick, Ph.D. thesis, Rice University, 1994.